

Constraining 20th-Century Sea-Level Rise in the South Atlantic Ocean

Thomas Frederikse, Surendra Adhikari, Tim Daley, Sönke Dangendorf, Roland Gehrels, Felix Landerer, Marta Marcos, Thomas Newton, Graham Rush, Aimée Slangen, et al.

▶ **To cite this version:**

Thomas Frederikse, Surendra Adhikari, Tim Daley, Sönke Dangendorf, Roland Gehrels, et al.. Constraining 20th-Century Sea-Level Rise in the South Atlantic Ocean. Journal of Geophysical Research. Oceans, 2021, 126 (3), 10.1029/2020JC016970 . hal-03485276

HAL Id: hal-03485276
https://hal.science/hal-03485276

Submitted on 12 Aug 2022

HAL is a multi-disciplinary open access archive for the deposit and dissemination of scientific research documents, whether they are published or not. The documents may come from teaching and research institutions in France or abroad, or from public or private research centers.

L'archive ouverte pluridisciplinaire **HAL**, est destinée au dépôt et à la diffusion de documents scientifiques de niveau recherche, publiés ou non, émanant des établissements d'enseignement et de recherche français ou étrangers, des laboratoires publics ou privés.

Copyright

Check for updates

JGR Oceans

RESEARCH ARTICLE
10.1029/2020JC016970

Constraining 20th-Century Sea-Level Rise in the South Atlantic Ocean

Thomas Frederikse[1], Surendra Adhikari[1], Tim J. Daley[2], Sönke Dangendorf[3,4], Roland Gehrels[5], Felix Landerer[1], Marta Marcos[6,7], Thomas L. Newton[2], Graham Rush[5], Aimée B. A. Slangen[8], and Guy Wöppelmann[9]

[1]Jet Propulsion Laboratory, California Institute of Technology, Pasadena, CA, USA, [2]School of Geography, Earth and Environmental Sciences, Plymouth University, Plymouth, UK, [3]Old Dominion University, Norfolk, VA, USA, [4]University of Siegen, Siegen, Germany, [5]Department of Environment and Geography, University of York, York, UK, [6]IMEDEA (UIB-CSIC), Esporles, Spain, [7]Department of Physics, University of the Balearic Islands, Palma, Spain, [8]Department of Estuarine and Delta Systems, NIOZ Royal Netherlands Institute for Sea Research, Utrecht University, Yerseke, The Netherlands, [9]LIENSs, Université de La Rochelle – CNRS, La Rochelle, France

Abstract Sea level in the South Atlantic Ocean has only been measured at a small number of tide-gauge locations, which causes considerable uncertainty in 20th-century sea-level trend estimates in this basin. To obtain a better-constrained sea-level trend in the South Atlantic Ocean, this study aims to answer two questions. The first question is: can we combine new observations, vertical land motion estimates, and information on spatial sampling biases to obtain a likely range of 20th-century sea-level rise in the South Atlantic? We combine existing observations with recovered observations from Dakar and a high-resolution sea-level reconstruction based on salt-marsh sediments from the Falkland Islands and find that the rate of sea-level rise in the South Atlantic has likely been between 1.1 and 2.2 mm year^{-1} (5%–95% confidence intervals), with a central estimate of 1.6 mm year^{-1}. This rate is on the high side, but not statistically different compared to global-mean trends from recent reconstructions. The second question is: are there any physical processes that could explain a large deviation from the global-mean sea-level trend in the South Atlantic? Sterodynamic (changes in ocean dynamics and steric effects) and gravitation, rotation, and deformation effects related to ice mass loss and land water storage have probably led to a 20th-century sea-level trend in the South Atlantic above the global mean. Both observations and physical processes thus suggest that 20th-century sea-level rise in the South Atlantic has been about 0.3 mm year^{-1} above the rate of global-mean sea-level rise, although even with the additional observations, the uncertainties are still too large to distinguish a statistically significant difference.

Plain Language Summary Before the satellite era, we depend on the tide-gauge network to measure sea-level changes. In the North Atlantic and Pacific Oceans, many tide gauges have been installed, but there are only a handful in the South Atlantic Ocean. Because of this, it is challenging to accurately determine 20th-century sea-level changes in the South Atlantic. Because the South Atlantic Ocean covers about one-fifth of the global oceans, estimates of global sea-level changes are also affected by the low number of observations in the South Atlantic. Here, we try to improve this situation by adding recently rescued tide-gauge observation data from Dakar and a new paleo record that has been derived from a salt marsh in the Falklands to the existing sea-level records. We find that since 1900, South Atlantic sea level has likely risen slightly faster than the global average. This above-average rate makes sense, because thermal expansion in the South Atlantic has likely been faster than the global mean, and mass loss from ice sheets and glaciers results in above-average sea-level rise in the South Atlantic.

Key Points:

- We estimate 20th-century sea-level changes in the South Atlantic Ocean from tide-gauge data and a new paleo proxy
- 20th-century sea-level rise in the South Atlantic might have been above the global mean, but uncertainties remain large
- Estimates of contemporary mass redistribution and sterodynamic effects support this above-average trend

Supporting Information:

Supporting Information may be found in the online version of this article.

Correspondence to:

T. Frederikse,
thomas.frederikse@jpl.nasa.gov

Citation:

Frederikse, T., Adhikari, S., Daley, T. J., Dangendorf, S., Gehrels, R., Landerer, F., et al. (2021). Constraining 20th-century sea-level rise in the South Atlantic Ocean. *Journal of Geophysical Research: Oceans*, *126*, e2020JC016970. https://doi.org/10.1029/2020JC016970

Received 9 NOV 2020
Accepted 19 FEB 2021

The copyright line for this article was changed on 01 JUL 2021 after original online publication.

© 2021. American Geophysical Union. All Rights Reserved.

1. Introduction

Reconstructions of global-mean sea level (GMSL) over the 20th-century are predominately based on tide-gauge observations, which are both sparse and unevenly distributed around the globe. The tide-gauge network consists of a limited number of records, most of which are found along the North American and European coastlines, while large parts of the oceans in the Southern Hemisphere are sparsely sampled (e.g., Jevrejeva et al., 2017; Woodworth et al., 2011). Since century-scale sea-level trends show a strong regional component (Kopp et al., 2015), this sparse sampling results in a considerable uncertainty in reconstructed

GMSL trends, which is difficult to quantify, since the causes and magnitude of these regional deviations are often unknown. Because all processes that cause sea-level changes have distinct spatial signatures, the sparse sampling could also result in biases in these reconstructions (Thompson et al., 2016). Among other factors, this uncertainty results in a spread between estimates of the rate of 20th-century sea-level rise: the central estimates in recent reconstructions varies from 1.3 to 2.0 mm year^{-1} between 1901 and 2010, with recent reconstructions (e.g., Dangendorf et al., 2017, 2019; Frederikse et al., 2020; Hay et al., 2015) tending toward lower trends than previously estimated (e.g., Church & White, 2011; Jevrejeva et al., 2014).

The South Atlantic Ocean is one of the most sparsely sampled oceans (Dangendorf et al., 2017). An analysis of the sea-level budget in this basin by Frederikse et al. (2018) points at a discrepancy between reconstructed sea-level changes and the estimated sum of contributing processes between 1958 and 2014: the reconstructed trend over 1958–2014 was 2.56 ± 0.47 mm year^{-1}, which was both significantly larger than the global-mean trend of 1.52 ± 0.19 mm year^{-1} and the sum of contributing processes in the South Atlantic, which was estimated at 1.58 ± 0.28 mm year^{-1}. The tide-gauge record in Buenos Aires is the only record that provides observations for the first half of the century, and for which estimates of vertical land motion (VLM) are available (Santamaría-Gómez et al., 2017). As a result, this station has a large influence on sea-level reconstructions, and errors and uncertainties will propagate into GMSL estimates with considerable weight. However, it is unknown how representative this station is for sea-level changes in the South Atlantic. The record also shows considerable interannual variability, which is not consistent with the low interannual variability in the South Atlantic Ocean that is expected from ocean dynamics models (Forget & Ponte, 2015). Furthermore, estimates of VLM in this area differ between nearby Global Navigation Satellite Systems (GNSS) stations, as well as between processing centers, although generally, they indicate an uplift signal (Santamaría-Gómez et al., 2017; Wöppelmann & Marcos, 2016). Therefore, to increase confidence in reconstructed sea-level changes in the South Atlantic, we have to overcome our dependence on this single tide-gauge record, and increase the number of sea-level observations that span the whole twentieth century.

An alternative to observation-based sea-level changes is to reconstruct sea level by quantifying and summing up all relevant physical processes that cause sea-level changes in the South Atlantic Ocean. Since for multiple processes no estimates of their contribution to 20th-century basin-mean sea level are available, which include the sterodynamic (i.e., the combined effects of ocean dynamics and global-mean steric sea-level changes) and the Antarctic Ice Sheet contribution, this approach is not feasible. However, we could determine whether there are processes that could likely cause a deviation between GMSL changes and sea-level changes in the South Atlantic Ocean over the 20th-century. Glacial Isostatic Adjustment (GIA) and present-day mass redistribution over the 20th-century cause changes in the geoid, Earth rotation and deformation (GRD), resulting in spatial sea-level and VLM patterns, which could cause such deviations on decadal and longer time scales (e.g., Spada, 2017). Ocean sterodynamic processes related to large-scale changes in the ocean temperature and salinity could also drive such deviations (e.g., Durack et al., 2014; Kopp et al., 2015). A similar process-based analysis was done by Thompson et al. (2016), who showed that many long tide-gauge records underestimate rather than overestimate the 20th-century global-mean sea-level trend.

In this study, we combine existing tide-gauge observations with a new long-term tide-gauge record from Dakar and a high-resolution salt-marsh record from the Falkland Islands (Newton, 2017; Newton et al., 2020) to estimate a likely range of 20th-century sea-level rise in the South Atlantic. With these new observations, we estimate 20th-century sea-level changes in the South Atlantic Ocean. Due to the new records, this estimate does not depend solely on the tide-gauge record of Buenos Aires to estimate the sea-level changes over the early decades of the 20th-century. We combine these in situ sea-level observations with local VLM observations and estimates of spatial sampling biases related to GRD effects due to GIA and present-day mass redistribution to reconstruct the 20th-century sea-level trend in this basin, together with an estimate of its uncertainty. We then use the process-based approach to determine whether there are known physical processes that could cause a difference between global and South Atlantic Ocean sea-level changes over the 20th-century.

The study is structured as follows: in Section 2, we introduce the data and methods. In Section 3, we discuss an array of tide-gauge observations to estimate a likely range of the trend that follows from the observations, and in Section 4, we discuss whether the effects of GIA, GRD effects due to present-day mass redistribution,

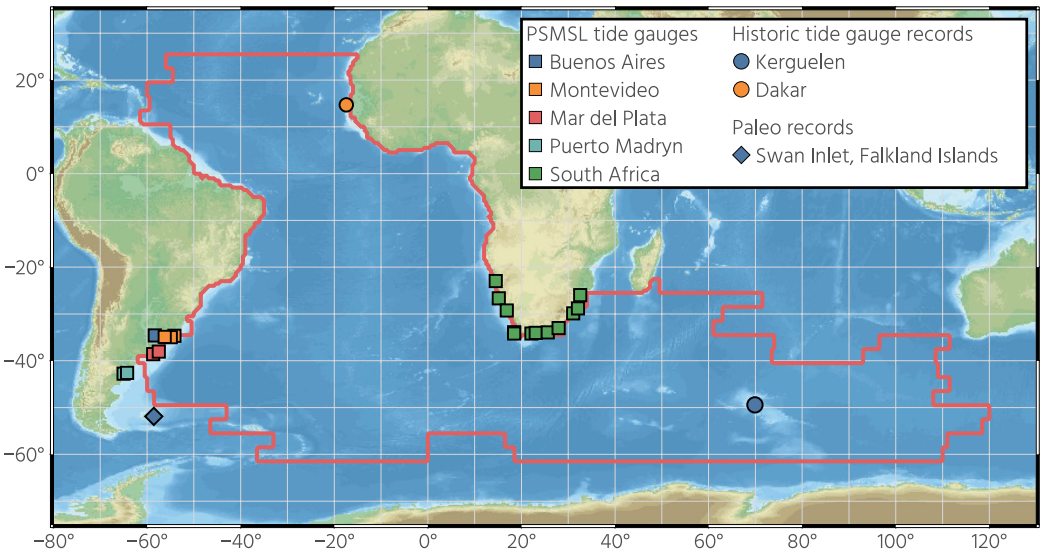


Figure 1. The locations of each region and the individual observations per region, as listed in Table 1. The red line denotes the boundary of the South Atlantic Ocean, as defined by Thompson and Merrifield (2014).

or ocean dynamics could explain a difference between the South Atlantic and GMSL, followed by the discussions and conclusions in Section 5. Note that in this study, we try to adhere to the sea-level terminology as proposed by Gregory et al. (2019), which introduces some of the terms that are used throughout this study.

2. Data and Methods

To obtain a consistent basin-mean sea-level curve, and to estimate basin-mean sea-level changes, we need a consistent definition of the basin. Here, we define the South Atlantic Ocean following the analysis of Thompson and Merrifield (2014), who split the global ocean in basins that show a common decadal sea-level variability signal. With this basin definition, which is depicted in Figure 1, parts of the classic Southern Ocean and Indian Ocean are part of the basin. This definition has two advantages over the use of the classic definition of the South Atlantic: the new domain is bounded by an extra historical tide-gauge record, and the basin shares a common variability signal. The same basin definitions were also used in the global 20th-century sea-level reconstructions from Dangendorf et al. (2017) and Frederikse et al. (2020), and the regional budget analysis in Frederikse et al. (2018).

2.1. GIA and GRD Effects due to Present-Day Mass Redistribution

GIA is the ongoing response of sea level, the Earth gravity field, Earth rotation parameters, and the solid Earth to the growth and deglaciation of the global ice sheets in the past. This response results in both local sea-level and solid-earth changes at the observation locations, as well as in large-scale effects, that could affect the basin as a whole. To estimate these effects, and to quantify the related uncertainty, we use 5,000 members of the large ensemble of GIA models computed by Caron et al. (2018). This ensemble is generated by perturbing the deglaciation histories and the solid-earth properties, and each ensemble member is attributed a likelihood by comparing the modeled changes to an array of paleo benchmarks and GNSS observations.

Present-day mass redistribution also causes GRD changes, which could affect local and basin-mean sea level. To estimate the effects of individual sources of ice mass loss on South Atlantic sea-level, we have computed the GRD effects from uniform mass loss from the Greenland Ice Sheet, the West and East Antarctic Ice Sheet, and from glaciers. For the latter, we determine the relative contribution of each glaciated region from the Randolph Glacier Inventory (Pfeffer et al., 2014) using the 20th-century regional estimates from Marzeion et al. (2015). We also estimate the total effect of present-day mass redistribution, based on

realistic estimates of ice mass loss and terrestrial water storage on sea-level changes in the South Atlantic. For this estimate, we use two datasets: the estimate compiled by Adhikari et al. (2018) and the estimate from Frederikse et al. (2020). Both sets contain realistic estimates of mass changes related to glaciers, ice sheets, terrestrial water storage related to the impoundment of water behind dams, and groundwater depletion, as well as an estimate of the uncertainties.

We solve the sea-level equation of an elastic and incompressible Earth using the pseudo-spectral method (Tamisiea et al., 2010) and include rotational feedback following Milne and Mitrovica (1998). We use elastic load Love numbers from Wang et al. (2012), which are based on the Preliminary Reference Earth Model (Dziewonski & Anderson, 1981).

2.2. Sterodynamic Changes and the CMIP5 Ensemble

Local sterodynamic sea-level variability can be separated into the steric part, which are local sea-level changes related to local density changes and the local ocean mass part, driven by ocean dynamics. The vast majority of the decadal sterodynamic sea-level variability and long-term trends in the South Atlantic Ocean are associated with density changes rather than local ocean mass changes (Forget & Ponte, 2015; Meyssignac et al., 2017; Piecuch et al., 2013). Therefore, we assume that estimates of temperature- and salinity-driven density changes can be used to assess basin-scale trends in sterodynamic sea level. We use gridded temperature and salinity estimates from four different sources covering the period 1957–2018: monthly data from EN4 version 4.2.1 (Cheng & Zhu, 2016; Good et al., 2013; Ishii et al., 2017). From these fields, we computed local steric anomalies using the TEOS-10 toolbox (McDougall & Barker, 2011), from which we compute linear trends over the 1957–2018 period. We also use the pentadal steric anomaly estimates from Levitus et al. (2012).

To further analyze whether sterodynamic processes could lead to basin-mean deviations on century time scales, we use the model estimates from Meyssignac et al. (2017) and Slangen et al. (2017), which are compiled from the Coupled Model Intercomparison Project 5 (CMIP5) global climate model ensemble. This database contains estimates of sterodynamic changes, changes due to GIA, and GRD effects due to present-day mass redistribution. The dataset has 12 ensemble members, from which we compute time series of 20th-century sea-level changes over the South Atlantic basin and over the global oceans. We consider both sterodynamic sea level and total sea level, which consists of sterodynamic changes, GIA, and GRD effects due to present-day mass redistribution.

2.3. Sea-Level Observations and Estimates of Vertical Land Motion

We use sea-level observations from tide gauges and a salt-marsh record from the Falkland Islands. All locations from which we use data are shown on the map in Figure 1. We use monthly tide-gauge data from the Permanent Service for Mean Sea-Level (Holgate et al., 2013; PSMSL, 2019), as well as historical observations from Dakar and Kerguelen Island, which have been the result of multiple data rescue efforts. Le Cozannet et al. (2015) analyzed the available data from Dakar from 1942 to 2012. This time series has been expanded and now covers large parts of the 20th-century, together with benchmark stability information. We use all available data between 1900 and 2010. For Kerguelen Island, we use the measurements from the data rescue effort by Testut et al. (2006), which is a synthesis of a year (1962) of tide pole readings and a decade (1994–2004) of hourly tide-gauge measurements separated by 3 decades without data. Testut et al. (2006) derived a linear trend of 1.1 mm year^{-1} between 1962 and 2004 from this record.

For the Falkland Islands, Newton (2017) and Newton et al. (2020) have produced a late Holocene sea-level reconstruction from the Swan Inlet salt marsh. From this record, we use the 15 sea-level index point that are dated within the 20th- and 21st-century. To the best of our knowledge no other suitable paleo records are available in this basin, besides the salt-marsh record in eastern South Africa (Strachan et al., 2014) which has too low a resolution to resolve recent sea-level changes. A full description of this salt-marsh reconstruction can be found in Newton (2017) and Newton et al. (2020), and we provide a summary below. Like other salt-marsh sea-level reconstructions (e.g., Kopp et al., 2016), the Falkland Islands record is based on the assumption that, over multiple decades, the sediment accretion rate in the salt marsh combined with

microfossil analyses of the sediments can be used as a proxy for sea-level rise (Gehrels, 2000). This approach requires that the sediments can be accurately dated, which was accomplished by a combination of ^{137}Cs and ^{14}C dating (supporting information S1), providing a 1,300-year long sea-level reconstruction from a 0.9 m sediment core (Newton, 2017). The 20th- and 21st-century part of the reconstruction is used here. This part consists of 15 index points, with a maximum time step of 10 years between two consecutive points. It is based on the top 0.15 m of the core and supported by ^{137}Cs (Figure S3) and ^{14}C (Table S3) measurements that provided an age-depth model for the core (Figure S4). Former heights of the salt-marsh surface relative to sea level were estimated from detailed analyses of microfossils (diatoms) preserved in the sediments (Figure S5; Table S1; Newton et al., 2020). To achieve this, the vertical distributions of the modern counterparts of the diatoms were first surveyed across Swan Inlet salt marsh, and their relationship with tidal elevations was quantified in regression equations (a "transfer function"; supporting information S1; Figures S1 and S2; Newton et al., 2020).

This transfer-function approach is widely used in proxy-based sea-level reconstructions (Barlow et al., 2013; Kopp et al., 2016). The Swan Inlet transfer function was subsequently applied to the microfossils in a sediment core to calculate former heights of sea level (supporting information S1, Table S2) spanning the period 1908–2006. For further details of the proxy sea-level reconstruction technique we refer to Newton et al. (2020) and to the supporting information (Birks, 1995; Blaauw & Christen, 2011; Brain et al., 2011; Juggins, 2003; Kemp & Telford, 2015; Shennan, 1986; Shennan et al., 2015; Watcham et al., 2013). Some index points have a higher dissimilarity coefficient to modern analogs. These points are depicted in light blue in Figure 2h. We have tested the effect of omitting these points, which only led to minor changes in the resulting 20th-century trends. See supporting information S1 for more details on this experiment. Figure 2h also depicts two tide-gauge records that are close to the Swan Inlet salt marsh: Port Louis and Port Stanley. Woodworth et al. (2010) have analyzed observations collected during individual campaigns in Port Louis, and Stanley features a permanent tide-gauge station listed on PSMSL. The tide-gauge data from both Port Louis and Port Stanley do not point at any large discrepancies with the index points. This agreement of the index points with the tide-gauge observations gives additional trust in the index points that have been dated after 1970, who generally have a relatively large minimum dissimilarity coefficient with modern analogs (Figure S5), which implies a larger uncertainty that is not directly quantifiable.

The time series of the sea-level observations at individual locations are merged into regions, which are listed in Table 1. For some regions, only one location with observation is available, and in that case, the observation at this single location is used as the regional estimate. For many regions, more than one record is available. To merge these multiple records into a single regional estimate, we apply the virtual station method (Dangendorf et al., 2017; Jevrejeva et al., 2014). First, we remove the seasonal cycle from the time series of each record, and then the time series from the two stations are subsequently averaged into a new time series at a virtual station until only one virtual station is left, which is used as the regional sea-level curve.

Tide gauges are referenced to a local stable benchmark, and therefore, two different tide gauges, which are each referenced to their own benchmark, cannot be combined without defining a common reference level. We estimate a common reference level by estimating mean sea level in both merged stations over the period where both stations provide observations. We subsequently adjust both records to this mean value. For the region estimates, we deviate from the original virtual station method: instead of subsequently merging the closest stations, we average the two stations with the longest common overlap period into a new virtual station. We have chosen this approach, since all merged stations are located close to each other, and maximizing the overlapping periods reduces the chance of drifts. The regions with the tide gauges that have been used to compute the region-averaged time series are listed in Table 1.

Since tide gauges are located on land, local VLM could affect the observations (Wöppelmann & Marcos, 2016). Therefore, we assess VLM at our observation locations using a combination of GNSS and Doppler Orbitography and Radiopositioning Integrated by Satellite (DORIS) observations. Due to solid-earth deformation caused by present-day mass redistribution, VLM derived over the short GNSS/DORIS records is not necessarily representative of the longer sea-level records (Riva et al., 2017). The coastal regions of South America are especially affected by solid-Earth deformation due to changes in terrestrial water storage, which could alias into the VLM trend when the VLM observations are not corrected (Frederikse et al., 2019).

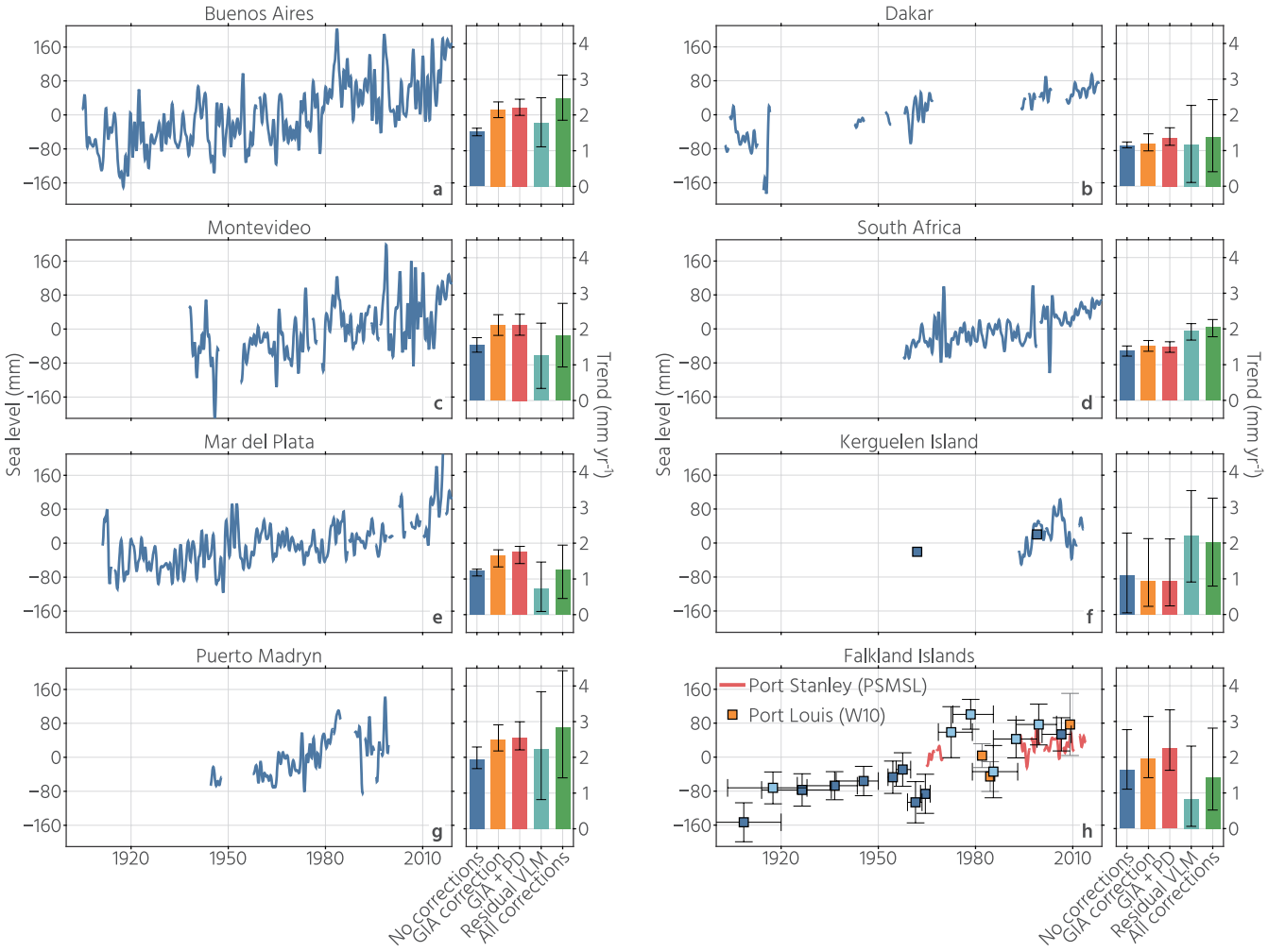


Figure 2. Estimates of sea-level changes and vertical land motion at each region. The left panels show the time series of the resulting RSL curve after merging the individual records into region estimates. For clarity, the individual time series have been low-pass filtered using a 13-month Butterworth filter. The right panel shows the estimates of the basin-mean sea-level trend using multiple spatial corrections, as described in Equation 1. The trends are computed over the periods for which a region provides observations. The error bars show the (5%–95%) confidence intervals. Panels a-g depict tide-gauge records. For the Falkland Islands proxy record (Panel h), the Port Stanley tide-gauge observations from PSMSL and Port Louis observations from Woodworth et al. (2010) are shown for comparison. The light blue dots in panel h refer to index point with a higher dissimilarity coefficient to modern analogs. The trends are also listed in Table S4. PSMSL, Permanent Service for Mean Sea Level.

To avoid this aliasing, we use an updated version of the GNSS dataset from Frederikse et al. (2019). This dataset uses GNSS data from the University of Nevada, Reno (UNR) database (Blewitt et al., 2018), from which solid-Earth deformation due to GIA and contemporary mass redistribution is subtracted. After this subtraction, local linear residual VLM trends are computed using the MIDAS approach (Blewitt et al., 2016). Note that the specific choice of the GNSS trend estimation approach could have an impact on the estimated linear trend (Santamaría-Gómez et al., 2017). We assume that the trend in residual VLM is predominantly driven by secular processes and is representative of the whole tide-gauge record. We apply the same approach to the DORIS data from Klos et al. (2017). For each tide-gauge location, we check all available GNSS stations within a 50 km radius for which at least 4 years of data is available, and for which the estimated uncertainty in the vertical trend is smaller than 2 mm year^{-1}. We have manually checked every GNSS station for spurious signals, and only include stations without obvious issues. Table 1 lists all the GNSS and DORIS stations used for each region. For regions with multiple VLM observations, the individual trends are averaged, weighted by the inverse of the standard error squared.

Table 1
Overview of Tide-Gauge and GNSS Stations Used for Each Region

Region	Time span	Completeness (%)	PSMSL id	GNSS code
Buenos Aires	1905–2018	99.5	157, 832	IGM1, BUE1, BUE2, MA02, LPGS
Montevideo	1938–2018	89.2	431, 434, 761	UYMO, MTV1, MTV2, UYLP
Mar del Plata	1910–2018	96.8	177, 223, 819, 857	BCAR, MPLA, MPL2
Puerto Madryn	1944–2000	72.7	501, 867	RWSN
Dakar	1902–2018	42.1	–	DAKR, DAKA, FG02
South Africa	1957–2018	98.4	284, 820, 826, 836, 910, 911, 914, 950, 1192, 1195	DRBA, DRBN, IXOP, PMBG, SCO1, STNG, PELB, CPNT, CTWN, HNUS, MALM, STBS, GEO1, GEOA, FG08, BISO, ELDN, WORC
Kerguelen	1962–1999	–	–	KERG, KRGG, KETG, KETB[a]
Falkland Islands	1908–2006	–	–	FALK, LKTH

For those regions based on tide-gauge time series, the completeness denotes the percentage of months within the time span for which observations are available. Note that for the Falklands and Kerguelen records, because of the use of index points instead of monthly data, no completeness has been listed. The PSMSL id denotes the station numbers as used by the Permanent Service for Mean Sea Level (PSMSL, Holgate et al., 2013), and the GNSS code refers to the codes for each GNSS station as used by Blewitt et al. (2018).

Abbreviations: DORIS, Doppler Orbitography and Radiopositioning Integrated by Satellite; GNSS, Global Navigation Satellite Systems.

[a]Denotes DORIS stations (Klos et al., 2017).

2.4. From Observations to a Basin-Mean Estimate

To constrain a likely basin-mean 20th-century trend range from the regional estimates, we have to consider that these estimates may be biased due the regional deviation from the basin-mean sea-level signals caused by GIA and GRD due to present-day mass redistribution, as well as due to local VLM. To remove these biases, we use the framework of Frederikse et al. (2018): for each region, we compute an estimate of basin-mean sea level, based on the regional sea-level observations and the difference between regional and basin-mean sea level due to GIA and present-day mass redistribution. This basin-mean estimate $\overline{\eta_i}$, based on sea-level observations η_i in region i reads

$$\overline{\eta_i} = \eta_i + R_{i,\text{residual}} + \overline{\eta_{\text{GIA}}} - \eta_{i,\text{GIA}} + \overline{\eta_{\text{PD}}} - \eta_{i,\text{PD}}. \quad (1)$$

here, all overlined terms denote basin-mean values. $R_{i,\text{residual}}$ denotes residual VLM in region i, and $\eta_{i,\text{GIA}}$ and $\eta_{i,\text{PD}}$ denote RSL changes related to GIA and GRD due to present-day mass changes in the region, while the overlined terms denote their basin-mean counterparts.

For each region in Table 1, we compute these basin estimates, as well as the accompanying uncertainties by generating 5,000 Monte Carlo ensembles. We start by estimating the properties of the serially correlated noise content of each regional estimate. We then generate 5,000 perturbed time series by simulating serially correlated Gaussian noise with the same properties. We use the Hector software (Bos et al., 2013) to estimate the noise properties of each regional sea-level curve, and to generate the artificial noise, which is added to the observed sea-level curve. We assume that for all regions, the noise spectrum can be described by a Generalized-Gauss-Markov model. This model generally performs well for sea-level data and avoids the possible over or underestimation of the temporal variability that could occur when using a first-order autoregressive noise model (Bos et al., 2014; Royston et al., 2018). For the salt-marsh data from Swan Inlet, Falkland Islands, we generate estimates by randomly perturbing both the time and height of each sea-level estimate following the estimated uncertainty in both. To be able to merge the salt-marsh and tide-gauge records, we interpolate each generated salt-marsh time series to monthly data. For Kerguelen Island, we perturb the estimated trend by the listed uncertainty. For the GIA term, we use an ensemble member, and for present-day mass GRD effects, we use the aforementioned reconstruction from Frederikse et al. (2020),

and perturb each local estimate using the accompanied uncertainty estimates. The residual VLM trend is also perturbed with a value that is derived from a Gaussian random number generator using the uncertainty estimate as the standard deviation of the generated noise. We use this ensemble of region estimates to derive a mean estimate of the trend, as well as the accompanying confidence intervals.

To average the time series from each region into one basin estimate, we again use the virtual station method. We start with the two stations that are closest to each other, which are averaged into one virtual station halfway. This procedure is repeated until one station is left, which we then use as our basin estimate. We repeat this procedure for each of the 5,000 regional sea-level curve ensemble members. This gives us 5,000 basin estimates. Similar to the region estimates, we use this ensemble to derive the trend and the accompanying confidence intervals. Note that with this procedure, we obtain a monthly basin-mean time series of basin-mean sea level. However, this reconstructed time series consists of monthly mean tide-gauge data, a 40-year linear trend from Kerguelen Island, and salt-marsh data that only contain information of longer-term sea-level changes, and as a result, the interannual and decadal variability in the resulting basin-mean curve has to be treated with caution. To avoid this issue, we only discuss the resulting trends over the period 1901–2010.

3. An Observation-Based Estimate of Sea-Level Rise in the South Atlantic

The time series and sea-level trends from each individual region are shown in Figure 2. Also shown are the estimates of the basin-mean sea-level trend from each record after applying one or more of the bias corrections from Equation 1.

The first region we analyze is Buenos Aires, whose time series is the longest available record in this basin from the PSMSL database, although it consists of two different tide gauges: Buenos Aires, operating between 1905 and 1987, and Palermo, which started in 1957, and is still operating today. When these stations are merged, they form a near-complete record covering almost the whole 20th-century. The record contains a considerable interannual variability signal, which is in contrast to what is expected for the nearby open ocean, where models suggest only a small variability signal at these time scales (Forget & Ponte, 2015). Given that the Rio de la Plata estuary, along which the Buenos Aires tide gauges are located, is the end point of the Uruguay and the Paraná rivers and local hydrographic properties are influenced by river outflow variability (Guerrero et al., 1997; Santamaria-Aguilar et al., 2017), water levels in the bay may be more representative for river-discharge effects rather than open-ocean variability. While the uncorrected trend in the merged record is 1.5 mm year^{-1}, the corrections for GIA and present-day mass GRD effects, as well as local residual VLM cause a basin estimate with a central value of 2.5 mm year^{-1} over the 20th-century. In the same region, Montevideo also provides a long record, covering 1938–2018. This record shows a similar variability signal as Buenos Aires, which is not surprising as both records are located along the same estuary.

The next region with a long time series is Mar del Plata, which consists of three individual records that have been merged into a single composite time series. One of these records (PSMSL id 177) is from the PSMSL "metric" database, which means that information on the vertical datum is absent. However, the trends over the common overlap period between this and the other records does not reveal any significant differences, and from a visual inspection, the metric record from station 177 does not seem to be contaminated with slippage or offset issues. The composite record offers a near-continuous record covering the vast majority of the 20th-century, with less decadal variability than the Buenos Aires record, which is probably due to the fact that this region is less affected by river outflow effects (Santamaria-Aguilar et al., 2017). Despite the short distance between both locations, both the uncorrected trends and the basin estimates are lower than the trend in Buenos Aires. Further South, we use the shorter record from Puerto Madryn, which shows similar trends to the Buenos Aires record, although the uncertainties for this location are greater, mostly due to its short length and the fact that the single available GNSS record comes with a large uncertainty.

On the other side of the South Atlantic, the Dakar record shows a trend that is close to the global mean, while the impact of the GIA and present-day mass GRD effects on the basin estimates are small as well. GNSS observations do not point to a large residual VLM signal. However, these estimates are based on GNSS records that come with a substantial uncertainty. Next to the GNSS stations that we use to estimate local VLM, the DORIS station DAKA also shows a small VLM signal (Klos et al., 2017), but again, there is no

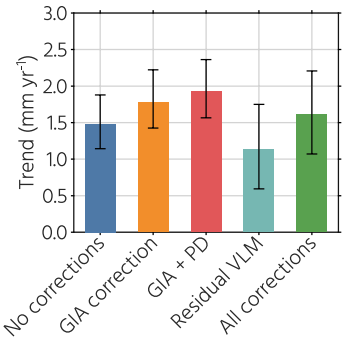


Figure 3. Estimates of the trend in sea level in the South Atlantic Ocean between 1901 and 2010 using various correction schemes, as described in Equation 1. The error bars show the (5%–95%) confidence intervals. The trends are also listed in Table S4.

overlap between the DORIS and the Gravity Recovery and Climate Experiment records to account for present-day mass redistribution effects. Also Le Cozannet et al. (2015) does not find any substantial VLM that could affect the tide-gauge record. The combination of the tide-gauge record with the GIA, contemporary mass, and residual VLM estimates results in a basin trend estimate with a central value of 1.4 mm year^{-1}.

For South Africa, residual VLM again results in a high basin estimate. This uplift signal is not based on a single GPS station, but is a common feature throughout Southern Africa, although this uplift cannot be related to any known elastic feature (Rodell et al., 2018). The large basin trends we obtain could be related to the strong warming signal related to the Agulhas Current and leakage, as discussed in Section 4.2.

For Kerguelen Island, we again find a smaller corrected and uncorrected trend, although the central estimate of the corrected trend is larger than most GMSL estimates. The Kerguelen record however, comes with an important caveat: since the record contains 30-year gap after 1 year of observations, the estimated trend could be affected by variability that aliased into these observations. While the uncertainty estimates of the trend do include an estimated contribution due to the aliasing of interannual variability, its magnitude remains poorly constrained (Testut et al., 2006).

Finally, the salt-marsh reconstruction from the Falkland Islands gives a central basin trend estimate of 1.5 mm year^{-1} ([5%–95%] confidence intervals 0.5–2.8 mm year^{-1}), despite the subsidence observed by the FALK GNSS station, which points at a residual VLM trend of −0.8 mm year^{-1}. There appears to be a noteworthy jump around the 1970s, which is not apparent from other records. Whether this is a local signal or a manifestation of the uncertainties in salt-marsh data is an open question. One possible cause could be the issue with the index points after the 1970s: they have a larger minimum dissimilarity coefficient with modern analogs, leading to larger uncertainties for these points.

From all regional estimates, we computed the likely range of the trend in sea-level rise in the South Atlantic between 1901 and 2010. Figure 3 shows that, using all corrections, we estimate a 20th-century sea-level trend of between 1.1 and 2.2 mm year^{-1} (5%–95% confidence intervals), with a best estimate of 1.6 mm year^{-1}. Both the GIA and contemporary GRD correction lead to a larger basin-mean trend estimate. While the best estimate without any bias corrections is 1.5 mm year^{-1}, including GIA results in an increase of 0.3 mm year^{-1}, while the correction for GIA, present-day mass changes and the residual VLM correction together result in an increase of 0.1 mm year^{-1}. The residual VLM correction reduces the basin-mean trend with 0.2 mm year^{-1}. This reduction can be traced back to the subsidence observed in Kerguelen, Mar del Plata, and the Falklands. However, the correction for local residual VLM has a large uncertainty due to the low number of observations. This uncertainty is the major reason for the large spread in reconstructed basin-mean sea-level changes.

4. Do Physical Processes Explain a Deviation From Global-Mean Sea-Level Rise in the South Atlantic Ocean?

The second question we want to answer is: are there known physical processes that could explain a deviation of the long-term sea-level trend in the South Atlantic from the global mean? Possible candidates that could result in a difference between global and basin-scale sea-level rise are GIA, GRD effects due to present-day mass redistribution, and sterodynamic changes in the ocean.

4.1. GIA and Present-Day Mass Redistribution

Figure 4 shows that the basin-mean sea-level change associated with GIA is −0.03 mm year^{-1}, which together with the small uncertainty of 0.02 mm year^{-1} effectively rules out that GIA is responsible for any large trend difference between the South Atlantic and the global mean. On the other hand, Figure 4 shows

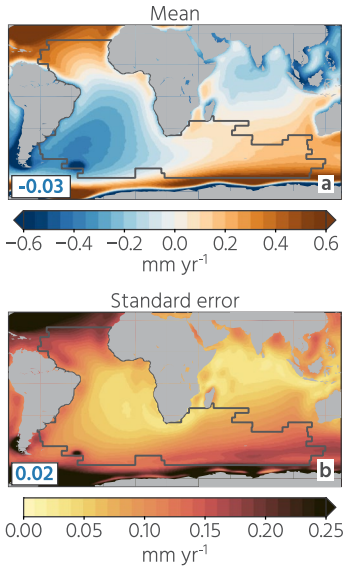


Figure 4. The impact of GIA on present-day relative sea level, based on the model ensemble from Caron et al. (2018). Panel (a) shows the mean, and the Panel (b) shows the standard error. The numbers in the lower-left corners denote the mean over the South Atlantic basin. GIA, Glacial Isostatic Adjustment.

a spatial pattern within the basin, with a sea-level drop along the American coast, and a rise at the South-eastern edge of the basin. As a result, while the basin-mean GIA signal is small, the signal is non-negligible at some of the observation locations. This effect can be seen in the Falkland Islands, Puerto Madryn, and Buenos Aires records, where the GIA correction has a large impact on the estimated trend (Figure 2).

Figure 5 shows that for all sources of ice mass loss, except for the East-Antarctic Ice Sheet, the South Atlantic Ocean will see a rise in sea level above the global average. The largest differences are found for the contribution of the Greenland Ice Sheet and glaciers. The only source for which the normalized fingerprint projects a below-average sea-level increase in the South Atlantic is the East-Antarctic Ice Sheet. This ice sheet is generally assumed to be in balance during the 20th-century and the first few years of the 21st century (Bamber et al., 2018; Shepherd et al., 2012), and it is unlikely that this ice sheet has contributed substantially to global and regional sea-level rise over the 20th-century. Therefore, the ice mass loss during the 20th-century will have caused an above-average sea-level rise in the South Atlantic, although the largest difference is 17% (Greenland), which could only explain deviations on the order of a tenth of a millimeter per year over the 20th-century. Similar to GIA, present-day mass redistribution could also cause significant sampling biases when basin-mean sea level is estimated from the sparse set of observations.

The deviation due to GRD effects from present-day mass redistribution is confirmed by the estimates from Adhikari et al. (2018) and Frederikse et al. (2020), which are depicted in Figure 6. Over the 20th-century, both these estimates show that sea-level rise in the South Atlantic due to barystatic processes has been above the global mean: Adhikari et al. (2018) shows a difference of 0.15 mm year^{-1}, while Frederikse et al. (2020) report 0.19 mm year^{-1}.

Taken together, GIA and GRD effects due to present-day mass redistribution are likely causing a sea-level rise in the South Atlantic that is larger than the GMSL rise, and its combined effect will be on the order of a few tenths of a millimeter per year.

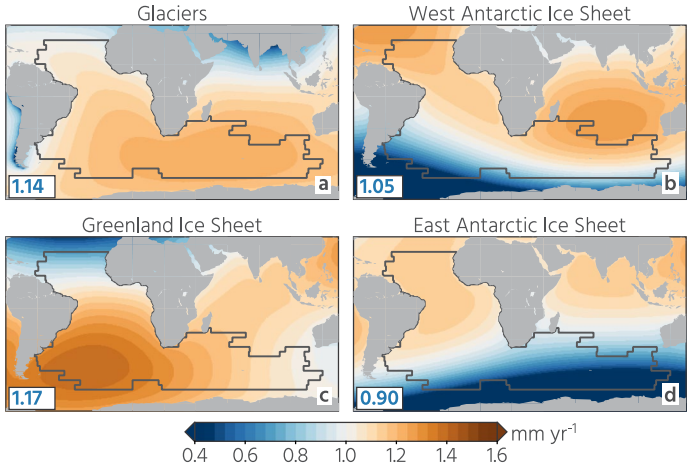


Figure 5. The spatial patterns of local relative sea-level changes associated with ice mass loss from glaciers (a), and spatially uniform mass loss Greenland Ice Sheet (c), and the West and East Antarctic Ice Sheet (b and d). The barystatic sea-level change is normalized to 1 mm year^{-1}. The blue number in the lower left corner shows the corresponding rate in the South Atlantic basin.

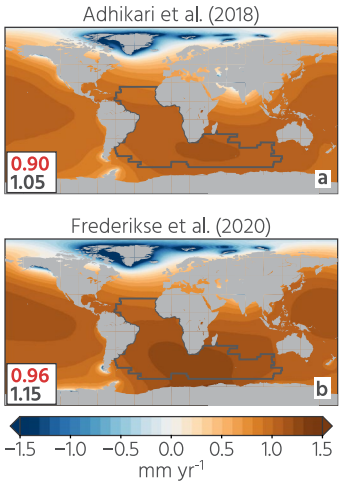


Figure 6. Relative sea-level changes associated with 20th-century mass redistribution estimated by Adhikari et al. (2018), Panel (a) and Frederikse et al. (2020), Panel (b). The estimate in Panel (a) is derived over 1901–2000, and the estimate in Panel (b) is computed over 1901–2018. The red number shows the global-mean trend, and the black number the trend (mm year^{-1}) averaged over the South Atlantic Ocean.

4.2. Sterodynamic Changes

The next candidate we investigate is the role of sterodynamic changes, which could cause basin-scale sea-level variability signals on decadal and multi-decadal time scales (Thompson & Merrifield, 2014). The resulting local, basin-mean and global steric trends, computed from in situ salinity and temperature observations between 1957 and 2018 are depicted in Figure 7. The steric reconstructions do not agree with each other on the spatial pattern of steric trends in the South Atlantic basin: for example the reconstruction from Cheng and Zhu (2016) and Ishii et al. (2017) show a stronger expansion in the South Atlantic interior, compared to EN4 and Levitus et al. (2012). It must be noted that before the Argo era (pre 2005), these reconstructions are based on manually collected temperature and salinity profiles, which have relatively sparse coverage in this basin (e.g., Johnson & Wijffels, 2011), that could result in biases in regional and basin-mean steric trends. Despite these uncertainties, there are common features visible in each of the reconstructions: Akin to the present-day mass redistribution case, in all reconstructions, the trend in the South Atlantic basin is larger than the global-mean trend. The difference is on the order of 0.2 mm year^{-1} and is driven by the fact that in this basin, a large heat uptake signals and accompanying thermosteric trend is only partially offset by freshening (Durack et al., 2014).

Despite the clustering approach to define the South Atlantic basin in such a way that it shows a common sea-level variability signal, the trends in steric sea level show spatial variability within the South Atlantic basin, with above-average trends along the South American coast and in the South-eastern part in each reconstruction, which may result in another deviation between local observations and basin-mean sea-level trends. Steric trends of more than 3 mm year^{-1} are found along the South African coastline. This coastline is affected by the Agulhas current and its leakage into the South Atlantic Ocean, and it is known that the sea water transported by this current shows rapid warming (Rouault et al., 2009), and as such, the above-average local sea-level observations from South Africa (Figure 2) may be caused by this rapid warming.

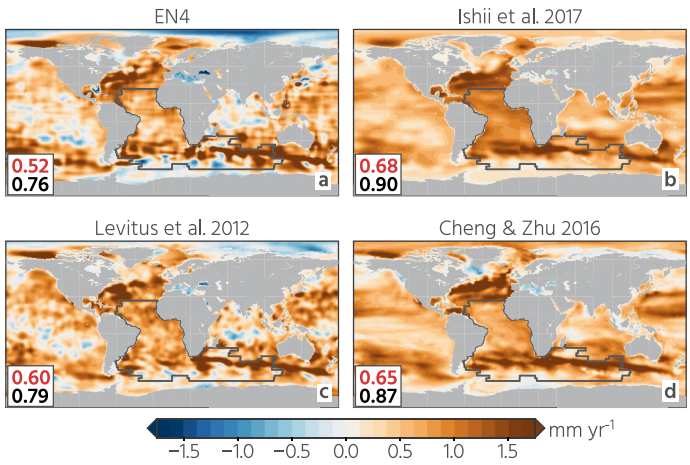


Figure 7. Trends in local steric sea level (1957–2018) from temperature and salinity observations, based on four reconstructions. The red number in each panel gives the global-mean trend in steric sea level, and the black number the basin-mean trend in the South Atlantic basin. The South Atlantic basin is denoted by the black contour. All units are mm year^{-1}. The global-mean steric trend is retained in the local and basin-mean estimates.

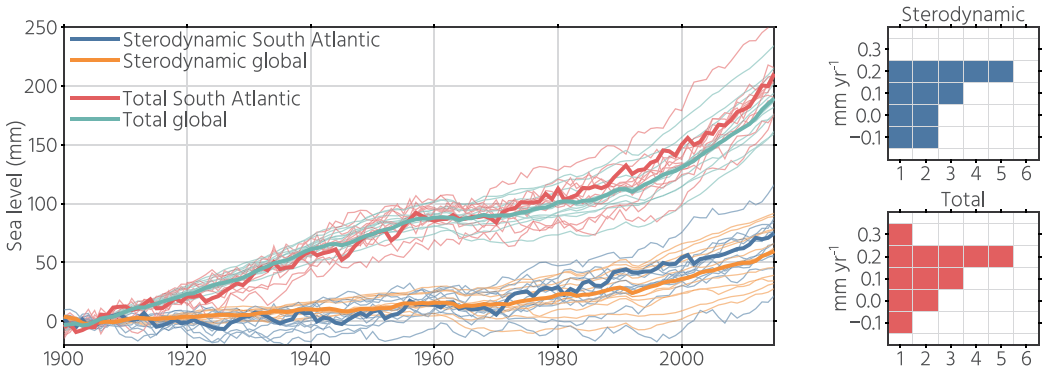


Figure 8. Global and South Atlantic sea-level changes of the 12-member historical CMIP5 model ensemble (Meyssignac et al., 2017; Slangen et al., 2017). Both the total sea level and the sterodynamic component are shown. Thin lines denote ensemble members, and thick lines denote the ensemble mean. The right panels show a histogram of the trend in the South Atlantic minus the global trend for total and dynamic sea level for each ensemble member. CMIP5, Coupled Model Intercomparison Project 5.

Figure 8 shows the results from this CMIP5 model ensemble (Meyssignac et al., 2017; Slangen et al., 2017): for both total and sterodynamic sea level, the ensemble mean shows a larger increase in sea level in the South Atlantic compared to the global ocean. To estimate the likely range of differences between the South Atlantic and GMSL, we computed the difference in the trend for each ensemble member. The results are plotted as a histogram in Figure 8. Most ensemble members show a rate that is on the order of a few tenths of a millimeter per year higher in the South Atlantic. This is the case for both the sterodynamic and the total changes. The latter is at odds with our conclusions from the previous section, which shows that sea-level changes driven by contemporary GRD effects in the South Atlantic are likely about 0.15 mm year^{-1} higher than for the global, while the CMIP5 ensemble shows a smaller GRD-induced difference. Possible reasons for this difference could be differences in the sea-level fingerprint computations and/or the use of different GIA models.

Both GRD effects and sterodynamic effects are likely to have caused an above-average sea-level change in the South Atlantic over the 20th-century, while the role of GIA is small. The magnitude of the difference between the 20th-century trend is in the order of a few tenths of millimeters per year. When we average the differences from the steric products that include temperature and salinity, and add these numbers to the GRD-induced difference, we obtain a difference between the South Atlantic and the global oceans of about 0.3 mm year^{-1} (Figure 9).

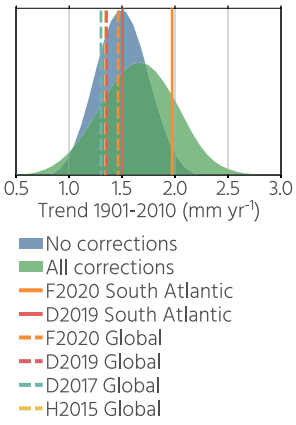


Figure 9. Comparison of the probability density function of the reconstructed trend in the South Atlantic using no corrections and all corrections, to the GMSL and South Atlantic trend from Dangendorf et al. (2019) (D2019), Frederikse et al. (2020) (F2020), and other recent GMSL reconstructions (Dangendorf et al., 2017, D2017; Hay et al., 2015, H2015). All trends have been computed over the period 1901–2010. GMSL, global-mean sea level.

5. Discussion and Conclusions

We reconstructed 20th-century South Atlantic sea-level rise using new observations from Dakar and the Falkland Islands, and used bias correction schemes to remove the sampling biases related to local VLM and GRD effects. Without these correction schemes, we find a reconstructed trend in the South Atlantic Ocean of 1.1–1.9 mm year^{-1}, with a central estimate of 1.5 mm year^{-1}. When we include these bias corrections, the reconstructed trend increases slightly to 1.1–2.2 mm year^{-1} with a central estimate of 1.6 mm year^{-1}. The central estimate is higher than most recent GMSL estimates, although the difference is not significant when taking the uncertainties into account (Dangendorf et al., 2017, 2019; Hay et al., 2015). The estimated basin-mean trends in the South Atlantic Ocean from Dangendorf et al. (2019) and Frederikse et al. (2020), are also greater than its estimated global-mean trend between 1901 and 2010 (1.95 vs. 1.45 mm year^{-1} and 1.50 vs. 1.35 year^{-1}, respectively).

This difference is not caused by a few individual regions, but all regional observations have a central basin trend in the South Atlantic above the global mean, except for Mar del Plata. The new records used in this study add additional evidence that the above-average central trend observed in the Buenos Aires record, which is the longest South Atlantic tide-gauge record in the PSMSL database, can also be found in other locations, although the central value of the estimated trend (2.5 mm year^{-1}) is higher than in the other long records in the South Atlantic.

The process-based approach also suggests that the 20th-century sea-level trend in the South Atlantic Ocean has been larger than the global-mean trend. Both steric expansion and present-day mass redistribution have contributed to this difference, each resulting in a difference on the order of 0.1–0.2 mm year^{-1}. Together, these processes result in a difference on the order of 0.3 mm year^{-1}, which is confirmed by results from CMIP5 models, although they project a smaller GRD-induced difference. GIA plays a minor role, although GIA does have an impact at specific tide-gauge sites within the South Atlantic basin. Both the observations and the process-based estimates point at an above-average sea-level rise in the South Atlantic Ocean of about 0.3 mm year^{-1}.

Even with the extra observations, the uncertainty is still large, and the difference with global-mean sea-level rise is not statistically significant. A part of this uncertainty is driven by VLM: estimating VLM trends from the short GNSS records introduces a large uncertainty, which affects the reconstructed trends. More GNSS records, or other VLM reconstruction methods, such as differenced tide gauge-altimetry trends (Wöppelmann & Marcos, 2016) and inSAR (Mahapatra et al., 2018) could improve this situation. One particular problem with GNSS records is the issue of the record length: trends estimated over the short GNSS record are assumed to hold over the complete tide-gauge records. This assumption does hold for many processes that cause VLM, such as sediment compaction, but other processes, such as tectonics and groundwater depletion can cause large short-term VLM signals (Wöppelmann & Marcos, 2016). Because the characteristics and causes of local VLM are often unknown, it is difficult to assess the error induced by this assumption. Some words of caution must also be added to our analysis of sterodynamic effects. First, the number of in situ temperature and salinity observations in the South Atlantic Ocean is limited, especially before the Argo era. The low number of observations affects all temperature and salinity datasets used in this study, and could cause an additional under or overestimation of the basin-mean trend (Abraham et al., 2013; Durack et al., 2014). Regional sterodynamic effects, such as the Agulhas current and leakage around South Africa, could cause regional biases, which have not been corrected for. From the observations, we cannot assess this spatial sampling bias, since ocean bottom pressure estimates in coastal locations are not available. At the coast, where the oceans are generally shallow, sterodynamic changes manifest mainly as bottom pressure signals (e.g., Bingham & Hughes, 2012), and sampling the steric fields at the tide-gauge locations is not a reliable estimator of this spatial bias. The comparison between observations and the CMIP5 model ensemble also comes with some limitations: this ensemble will not reproduce the internal variability in sea level, which could affect trends on decadal to centennial scales (e.g., Dangendorf et al., 2014). Furthermore, many processes that affect coastal sea level are not fully resolved in coarse-resolution ocean models, which could explain some of the differences between observed local tide-gauge trends and model results (Meyssignac et al., 2017; Slangen et al., 2017).

Even with the added records, the number of sea-level observations in the South Atlantic Ocean remains small, especially over the first half of the 20th-century, and large parts of the basin interior and many coastlines are still not covered by any observation (Marcos et al., 2019). Therefore, the spatial and temporal coverage of the observations remains sparse. Despite the addition of the Falklands record and the rescued tide-gauge data from Dakar, sea-level changes in the South Atlantic over the first half of the 20th-Century are based on only four records, which still results in a large uncertainty in basin-mean sea-level changes. Adding more regional sea-level observations to the basin-mean estimate could also reduce the uncertainties. We have omitted some long tide-gauge records from our analysis, mostly because of the presence of spurious trends and variability (most notably Cananeia and Ilha Fiscal in Rio de Janeiro), or the lack of reliable GNSS estimates, such as Takoradi. To test whether adding these stations affects our conclusions, we have estimated the basin-mean trend by including the both tide-gauge records under the assumption of no residual VLM. Adding these regions did not significantly change 20th-century trend (it stays at 1.6 mm year^{-1}) compared to our analysis based on stations for which VLM estimates are available. Some locations

in the PSMSL database also have longer records for which no datum information is available ("metric data") and for which no nearby records can be used as "buddy check," for example the Santos record near Sao Paolo, which has 56 years of data. An analysis on the reliability of these records, as well as data rescue projects and paleo proxies could all help to improve this situation.

Our understanding could also be improved by applying more sophisticated methods to determine the size of the spatial sampling bias due to sterodynamic processes. Given that the South Atlantic basin, as defined by Thompson and Merrifield (2014) covers 22% of the global oceans, this uncertainty affects global-mean sea-level reconstructions, and further reducing it may be one of the keys steps to reduce the spread among the various reconstruction techniques.

Data Availability Statement

The time series from Swan Inlet, the uniform GRD fingerprints from Figure 5, the steric estimates from Figure 7, and the scripts to compute all the results are available from https://doi.org/10.5281/zenodo.4542572.

Acknowledgments
The idea for this study emerged from the project "Towards a Unified Sea-Level Record: Assessing the Performance of Global-Mean Sea-Level Reconstructions from Satellite Altimetry, Tide Gauges, Paleo-Proxies and Geophysical Models," which was funded by the International Space Science Institute (ISSI), Bern Switzerland. Part of this work was carried out at the Jet Propulsion Laboratory, California Institute of Technology, under a contract with the National Aeronautics and Space Administration. Radiocarbon dating for the Falkland Islands proxy sea-level record was supported by the Natural Environment Research Council Radiocarbon Facility through allocation 1885.0415 (to RG). The authors thank Mark Garnett for help with the interpretation of the chronology and also thank the South Atlantic Environmental Research Institute (SAERI) for logistical support during our stay in the Falkland Islands. SONEL (www.sonel.org) observing system and its associated partners are acknowledged for recovering and making available the historical tide-gauge record of Dakar (and are encouraged to continue the data rescue endeavor). The authors would like to thank Phil Woodworth for sharing the datum information for the Falklands tide-gauge records and Ed Garrett for assisting in the uncertainty analysis of the Swan Inlet data.

References

Abraham, J. P., Baringer, M., Bindoff, N. L., Boyer, T., Cheng, L. J., Church, J. A., et al. (2013). A review of global ocean temperature observations: Implications for ocean heat content estimates and climate change. *Reviews of Geophysics*, *51*, 450–483. https://doi.org/10.1002/rog.20022

Adhikari, S., Caron, L., Steinberger, B., Reager, J. T., Kjeldsen, K. K., Marzeion, B., et al. (2018). What drives 20th century polar motion? *Earth and Planetary Science Letters*, *502*, 126–132. https://doi.org/10.1016/j.epsl.2018.08.059

Bamber, J. L., Westaway, R. M., Marzeion, B., & Wouters, B. (2018). The land ice contribution to sea level during the satellite era. *Environmental Research Letters*, *13*(6), 063008. https://doi.org/10.1088/1748-9326/aac2f0

Barlow, N. L., Shennan, I., Long, A. J., Gehrels, W. R., Saher, M. H., Woodroffe, S. A., & Hillier, C. (2013). Salt marshes as late Holocene tide gauges. *Global and Planetary Change*, *106*, 90–110. https://doi.org/10.1016/j.gloplacha.2013.03.003

Bingham, R. J., & Hughes, C. W. (2012). Local diagnostics to estimate density-induced sea level variations over topography and along coastlines. *Journal of Geophysical Research*, *117*(C1). https://doi.org/10.1029/2011JC007276

Birks, H. (1995). Quantitative palaeoenvironmental reconstructions. In D. Maddy, & J. Brew (Eds.), *Statistical modeling of quaternary science data* (pp. 161–254) Technical Guide 5. Quaternary Research Association.

Blaauw, M., & Christen, J. A. (2011). Flexible paleoclimate age-depth models using an autoregressive gamma process. *Bayesian Analysis*, *6*(3), 457–474. https://doi.org/10.1214/11-BA618

Blewitt, G., Hammond, W., & Kreemer, C. (2018). Harnessing the GPS data explosion for interdisciplinary science. *Eos*, *99*. https://doi.org/10.1029/2018EO104623

Blewitt, G., Kreemer, C., Hammond, W. C., & Gazeaux, J. (2016). MIDAS robust trend estimator for accurate GPS station velocities without step detection. *Journal of Geophysical Research: Solid Earth*, *121*, 2054–2068. https://doi.org/10.1002/2015JB012552

Bos, M. S., Fernandes, R. M. S., Williams, S. D. P., & Bastos, L. (2013). Fast error analysis of continuous GNSS observations with missing data. *Journal of Geodesy*, *87*(4), 351–360. https://doi.org/10.1007/s00190-012-0605-0

Bos, M. S., Williams, S. D. P., Araújo, I. B., & Bastos, L. (2014). The effect of temporal correlated noise on the sea level rate and acceleration uncertainty. *Geophysical Journal International*, *196*(3), 1423–1430. https://doi.org/10.1093/gji/ggt481

Brain, M. J., Long, A. J., Petley, D. N., Horton, B. P., & Allison, R. J. (2011). Compression behavior of minerogenic low energy intertidal sediments. *Sedimentary Geology*, *233*(1–4), 28–41. https://doi.org/10.1016/j.sedgeo.2010.10.005

Caron, L., Ivins, E. R., Larour, E., Adhikari, S., Nilsson, J., & Blewitt, G. (2018). GIA model statistics for GRACE hydrology, cryosphere, and ocean science. *Geophysical Research Letters*, *45*, 2203–2212. https://doi.org/10.1002/2017GL076644

Cheng, L., & Zhu, J. (2016). Benefits of CMIP5 multi-model ensemble in reconstructing historical ocean subsurface temperature variations. *Journal of Climate*, *29*(15), 5393–5416. https://doi.org/10.1175/JCLI-D-15-0730.1

Church, J. A., & White, N. J. (2011). Sea-level rise from the late 19th to the early 21st century. *Surveys in Geophysics*, *32*(4–5), 585–602. https://doi.org/10.1007/s10712-011-9119-1

Dangendorf, S., Hay, C., Calafat, F. M., Marcos, M., Piecuch, C. G., Berk, K., & Jensen, J. (2019). Persistent acceleration in global sea-level rise since the 1960s. *Nature Climate Change*, *9*, 705–710. https://doi.org/10.1038/s41558-019-0531-8

Dangendorf, S., Marcos, M., Wöppelmann, G., Conrad, C. P., Frederikse, T., & Riva, R. (2017). Reassessment of 20th century global mean sea level rise. *Proceedings of the National Academy of Sciences*, *114*(23), 5946–5951. https://doi.org/10.1073/pnas.1616007114

Dangendorf, S., Rybski, D., Mudersbach, C., Müller, A., Kaufmann, E., Zorita, E., & Jensen, J. (2014). Evidence for long-term memory in sea level. *Geophysical Research Letters*, *41*, 5530–5537. https://doi.org/10.1002/2014GL060538

Durack, P. J., Wijffels, S. E., & Gleckler, P. J. (2014). Long-term sea-level change revisited: The role of salinity. *Environmental Research Letters*, *9*(11), 114017. https://doi.org/10.1088/1748-9326/9/11/114017

Dziewonski, A. M., & Anderson, D. L. (1981). Preliminary reference Earth model. *Physics of the Earth and Planetary Interiors*, *25*(4), 297–356. https://doi.org/10.1016/0031-9201(81)90046-7

Forget, G., & Ponte, R. M. (2015). The partition of regional sea level variability. *Progress in Oceanography*, *137*, 173–195. https://doi.org/10.1016/j.pocean.2015.06.002

Frederikse, T., Jevrejeva, S., Riva, R. E. M., & Dangendorf, S. (2018). A consistent sea-level reconstruction and its budget on basin and global scales over 1958–2014. *Journal of Climate*, *31*(3), 1267–1280. https://doi.org/10.1175/JCLI-D-17-0502.1

Frederikse, T., Landerer, F., Caron, L., Adhikari, S., Parkes, D., Humphrey, V. W., et al. (2020). The causes of sea-level rise since 1900. *Nature*, *584*(7821), 393–397. https://doi.org/10.1038/s41586-020-2591-3

Frederikse, T., Landerer, F. W., & Caron, L. (2019). The imprints of contemporary mass redistribution on local sea level and vertical land motion observations. *Solid Earth*, *10*(6), 1971–1987. https://doi.org/10.5194/se-10-1971-2019

Gehrels, W. R. (2000). Using foraminiferal transfer functions to produce high-resolution sea-level records from salt-marsh deposits, Maine, USA. *The Holocene*, *10*(3), 367–376. https://doi.org/10.1191/095968300670746884

Good, S. A., Martin, M. J., & Rayner, N. A. (2013). EN4: Quality controlled ocean temperature and salinity profiles and monthly objective analyses with uncertainty estimates. *Journal of Geophysical Research: Oceans*, *118*, 6704–6716. https://doi.org/10.1002/2013JC009067

Gregory, J. M., Griffies, S. M., Hughes, C. W., Lowe, J. A., Church, J. A., Fukimori, I., et al. (2019). Concepts and terminology for sea level: Mean, variability and change, both local and global. *Surveys in Geophysics*, *40*, 1251–1289. https://doi.org/10.1007/s10712-019-09525-z

Guerrero, R. A., Acha, E. M., Framinan, M. B., & Lasta, C. A. (1997). Physical oceanography of the Río de la Plata Estuary, Argentina. *Continental Shelf Research*, *17*(7), 727–742. https://doi.org/10.1016/S0278-4343(96)00061-1

Hay, C. C., Morrow, E., Kopp, R. E., & Mitrovica, J. X. (2015). Probabilistic reanalysis of twentieth-century sea-level rise. *Nature*, *517*(7535), 481–484. https://doi.org/10.1038/nature14093

Holgate, S. J., Matthews, A., Woodworth, P. L., Rickards, L. J., Tamisiea, M. E., Bradshaw, E., et al. (2013). New data systems and products at the permanent service for mean sea level. *Journal of Coastal Research*, *288*, 493–504. https://doi.org/10.2112/JCOASTRES-D-12-00175.1

Ishii, M., Fukuda, Y., Hirahara, S., Yasui, S., Suzuki, T., & Sato, K. (2017). Accuracy of global upper ocean heat content estimation expected from present observational data sets. *Scientific Online Letters on the Atmosphere*, *13*, 163–167. https://doi.org/10.2151/sola.2017-030

Jevrejeva, S., Matthews, A., & Slangen, A. (2017). The twentieth-century sea level budget: Recent progress and challenges. *Surveys in Geophysics*, *38*(1), 295–307. https://doi.org/10.1007/s10712-016-9405-z

Jevrejeva, S., Moore, J., Grinsted, A., Matthews, A., & Spada, G. (2014). Trends and acceleration in global and regional sea levels since 1807. *Global and Planetary Change*, *113*, 11–22. https://doi.org/10.1016/j.gloplacha.2013.12.004

Johnson, G., & Wijffels, S. (2011). Ocean density change contributions to sea level rise. *Oceanography*, *24*(2), 112–121. https://doi.org/10.5670/oceanog.2011.31

Juggins, S. (2003). *C2 User Guide. Software for ecological and palaeoecological data analysis and visualisation, Technical Report*. Newcastle-upon-Tyne: University of Newcastle.

Kemp, A. C., & Telford, R. J. (2015). Transfer functions. In I. Shennan, A. J. Long, & B. P. Horton (Eds.), *Handbook of sea-level research* (pp. 470–499). Chichester: John Wiley & Sons, Ltd. https://doi.org/10.1002/9781118452547.ch31

Klos, A., Bogusz, J., & Moreaux, G. (2017). Stochastic models in the DORIS position time series: Estimates for IDS contribution to ITRF2014. *Journal of Geodesy*, *92*, 743–763. https://doi.org/10.1007/s00190-017-1092-0

Kopp, R. E., Hay, C. C., Little, C. M., & Mitrovica, J. X. (2015). Geographic variability of sea-level change. *Current Climate Change Reports*, *1*(3), 192–204. https://doi.org/10.1007/s40641-015-0015-5

Kopp, R. E., Kemp, A. C., Bittermann, K., Horton, B. P., Donnelly, J. P., Gehrels, W. R., et al. (2016). Temperature-driven global sea-level variability in the Common Era. *Proceedings of the National Academy of Sciences*, *113*(11), E1434–E1441. https://doi.org/10.1073/pnas.1517056113

Le Cozannet, G., Raucoules, D., Wöppelmann, G., Garcin, M., Da Sylva, S., Meyssignac, B., et al. (2015). Vertical ground motion and historical sea-level records in Dakar (Senegal). *Environmental Research Letters*, *10*(8), 084. https://doi.org/10.1088/1748-9326/10/8/084016

Levitus, S., Antonov, J. I., Boyer, T. P., Baranova, O. K., Garcia, H. E., Locarnini, R. A., et al. (2012). World ocean heat content and thermosteric sea level change (0–2,000 m), 1955–2010. *Geophysical Research Letters*, *39*(10). https://doi.org/10.1029/2012GL051106

Mahapatra, P., van der Marel, H., van Leijen, F., Samiei-Esfahany, S., Klees, R., & Hanssen, R. (2018). InSAR datum connection using GNSS-augmented radar transponders. *Journal of Geodesy*, *92*(1), 21–32. https://doi.org/10.1007/s00190-017-1041-y

Marcos, M., Wöppelmann, G., Matthews, A., Ponte, R. M., Birol, F., Ardhuin, F., et al. (2019). Coastal sea level and related fields from existing observing systems. *Surveys in Geophysics*, *40*, 1293–1317. https://doi.org/10.1007/s10712-019-09513-3

Marzeion, B., Leclercq, P. W., Cogley, J. G., & Jarosch, A. H. (2015). Brief Communication: Global reconstructions of glacier mass change during the 20th century are consistent. *The Cryosphere*, *9*(6), 2399–2404. https://doi.org/10.5194/tc-9-2399-2015

McDougall, T. J., & Barker, P. M. (2011). *Getting started with TEOS-10 and the Gibbs Seawater (GSW) oceanographic toolbox*. BatteryPoint: Trevor J McDougall.

Meyssignac, B., Slangen, A. B. A., Melet, A., Church, J. A., Fettweis, X., Marzeion, B., et al. (2017). Evaluating model simulations of twentieth-century sea-level rise. Part II: Regional sea-level changes. *Journal of Climate*, *30*, 8565–8593.

Milne, G. A., & Mitrovica, J. X. (1998). Postglacial sea-level change on a rotating Earth. *Geophysical Journal International*, *133*(1), 1–19. https://doi.org/10.1046/j.1365-246X.1998.1331455.x

Newton, T. L. (2017). *Holocene sea-level changes in the Falkland Islands: New insights into accelerated sea-level rise in the 20th Century* (PhD Thesis). The University of Plymouth.

Newton, T. L., Gehrels, W. R., Fyfe, R. M., & Daley, T. J. (2020). Reconstructing Sea-level change in the Falkland Islands (Islas Malvinas) using salt-marsh foraminifera, diatoms and testate amoebae. *Marine Micropaleontology*, *162*, 101923. https://doi.org/10.1016/j.marmicro.2020.101923

Pfeffer, W. T., Arendt, A. A., Bliss, A., Bolch, T., Cogley, J. G., Gardner, A. S., et al. (2014). The Randolph Glacier Inventory: A globally complete inventory of glaciers. *Journal of Glaciology*, *60*(221), 537–552. https://doi.org/10.3189/2014JoG13J176

Piecuch, C. G., Quinn, K. J., & Ponte, R. M. (2013). Satellite-derived interannual ocean bottom pressure variability and its relation to sea level. *Geophysical Research Letters*, *40*, 3106–3110. https://doi.org/10.1002/grl.50549

PSMSL. (2019). *Permanent Service for mean sea level*. Retrieved from http://www.psmsl.org/data/obtaining/

Riva, R. E. M., Frederikse, T., King, M. A., Marzeion, B., & van den Broeke, M. R. (2017). Brief communication: The global signature of post-1900 land ice wastage on vertical land motion. *The Cryosphere*, *11*(3), 1327–1332. https://doi.org/10.5194/tc-11-1327-2017

Rodell, M., Famiglietti, J. S., Wiese, D. N., Reager, J. T., Beaudoing, H. K., Landerer, F. W., & Lo, M.-H. (2018). Emerging trends in global freshwater availability. *Nature*, *557*, 651–659. https://doi.org/10.1038/s41586-018-0123-1

Rouault, M., Penven, P., & Pohl, B. (2009). Warming in the Agulhas Current system since the 1980's. *Geophysical Research Letters*, *36*(12), L12602. https://doi.org/10.1029/2009GL037987

Royston, S., Watson, C. S., Legrésy, B., King, M. A., Church, J. A., & Bos, M. S. (2018). Sea-level trend uncertainty with pacific climatic variability and temporally-correlated noise. *Journal of Geophysical Research: Oceans*, *123*, 1978–1993. https://doi.org/10.1002/2017JC013655

Santamaria-Aguilar, S., Schuerch, M., Vafeidis, A. T., & Carretero, S. C. (2017). Long-term trends and variability of water levels and tides in Buenos Aires and Mar del Plata, Argentina. *Frontiers in Marine Science*, *4*. https://doi.org/10.3389/fmars.2017.00380

Santamaría-Gómez, A., Gravelle, M., Dangendorf, S., Marcos, M., Spada, G., & Wöppelmann, G. (2017). Uncertainty of the 20th century sea-level rise due to vertical land motion errors. *Earth and Planetary Science Letters*, *473*, 24–32. https://doi.org/10.1016/j.epsl.2017.05.038

Shennan, I. (1986). Flandrian sea-level changes in the Fenland. II: Tendencies of sea-level movement, altitudinal changes, and local and regional factors. *Journal of Quaternary Science*, *1*(2), 155–179. https://doi.org/10.1002/jqs.3390010205

Shennan, I., Long, A. J., & Horton, B. P. (Eds.) (2015). *Handbook of Sea-Level Research: Shennan*. Chichester: John Wiley & Sons, Ltd. https://doi.org/10.1002/9781118452547

Shepherd, A., Ivins, E. R., Geruo, A., Barletta, V. R., Bentley, M. J., Bettadpur, S., et al. (2012). A reconciled estimate of ice-sheet mass balance. *Science*, *338*(6111), 1183–1189. https://doi.org/10.1126/science.1228102

Slangen, A. B. A., Meyssignac, B., Agosta, C., Champollion, N., Church, J. A., Fettweis, X., et al. (2017). Evaluating model simulations of twentieth-century sea level rise. Part I: Global mean sea level change. *Journal of Climate*, *30*(21), 8539–8563. https://doi.org/10.1175/JCLI-D-17-0110.1

Spada, G. (2017). Glacial isostatic adjustment and contemporary sea level rise: An overview. *Surveys in Geophysics*, *38*(1), 153–185. https://doi.org/10.1007/s10712-016-9379-x

Strachan, K. L., Finch, J. M., Hill, T., & Barnett, R. L. (2014). A late Holocene sea-level curve for the east coast of South Africa. *South African Journal of Science*, *110*(1/2), 1–9. https://doi.org/10.1590/sajs.2014/20130198

Tamisiea, M. E., Hill, E. M., Ponte, R. M., Davis, J. L., Velicogna, I., & Vinogradova, N. T. (2010). Impact of self-attraction and loading on the annual cycle in sea level. *Journal of Geophysical Research*, *115*(C7). https://doi.org/10.1029/2009JC005687

Testut, L., Wöppelmann, G., Simon, B., & Téchiné, P. (2006). The sea level at Port-aux-Français, Kerguelen Island, from 1949 to the present. *Ocean Dynamics*, *56*(5–6), 464–472. https://doi.org/10.1007/s10236-005-0056-8

Thompson, P. R., Hamlington, B. D., Landerer, F. W., & Adhikari, S. (2016). Are long tide gauge records in the wrong place to measure global mean sea level rise? *Geophysical Research Letters*, *43*, 10403–10411. https://doi.org/10.1002/2016GL070552

Thompson, P. R., & Merrifield, M. A. (2014). A unique asymmetry in the pattern of recent sea level change. *Geophysical Research Letters*, *41*, 7675–7683. https://doi.org/10.1002/2014GL061263

Wang, H., Xiang, L., Jia, L., Jiang, L., Wang, Z., Hu, B., & Gao, P. (2012). Load Love numbers and Green's functions for elastic Earth models PREM, iasp91, ak135, and modified models with refined crustal structure from Crust 2.0. *Computers & Geosciences*, *49*, 190–199. https://doi.org/10.1016/j.cageo.2012.06.022

Watcham, E. P., Shennan, I., & Barlow, N. L. M. (2013). Scale considerations in using diatoms as indicators of sea-level change: Lessons from Alaska. *Journal of Quaternary Science*, *28*(2), 165–179. https://doi.org/10.1002/jqs.2592

Woodworth, P., Gehrels, W. R., & Nerem, S. (2011). Nineteenth and twentieth century changes in sea level. *Oceanography*, *24*(2), 80–93. https://doi.org/10.5670/oceanog.2011.29

Woodworth, P. L., Pugh, D. T., & Bingley, R. M. (2010). Long-term and recent changes in sea level in the Falkland Islands. *Journal of Geophysical Research*, *115*(C9). https://doi.org/10.1029/2010JC006113

Wöppelmann, G., & Marcos, M. (2016). Vertical land motion as a key to understanding sea level change and variability. *Reviews of Geophysics*, *54*, 64–92. https://doi.org/10.1002/2015RG000502